Dormant Neutron Stars in the Milky Way

The Final Evolutionary Phase and Galactic Population Constraints

Boris Kriger
Institute of Integrative and Interdisciplinary Research
boriskriger@interdisciplinary-institute.org

April 2025 (Revised January 2026)

Abstract

Neutron stars that have exhausted their rotational and magnetic energy represent a theoretically predicted but observationally elusive population. While the ATNF Pulsar Catalogue lists ∼3,500 rotation-powered pulsars, population synthesis models predict $N_{\rm NS} \sim (1\text{–}2) \times 10^8$ neutron stars in the Milky Way, with systematic uncertainties of a factor of ∼2–3 arising primarily from supernova rate estimates, initial mass function slope variations, and neutron star retention fractions. We distinguish dormant neutron stars—which emit no detectable radiation at any wavelength—from radio-quiet but thermally emitting isolated neutron stars (XDINSs). This review examines the physical mechanisms rendering neutron stars undetectable: magnetic dipole spin-down, field decay via ohmic dissipation and Hall drift, and thermal cooling. We present quantitative detection thresholds: a 1.4 $M_\odot$ neutron star at 100 pc with surface temperature $T_s < 10^4$ K produces thermal flux below JWST MIRI sensitivity (∼10–100 nJy in deep exposures). Indirect detection via gravitational microlensing—constrained by OGLE/EROS surveys toward the Magellanic Clouds to $f_{\rm compact} \lesssim 10\%$ of halo mass for $M \sim 0.1\text{–}30\ M_\odot$—and accretion-induced reactivation offer viable pathways for disk/bulge populations. The total baryonic mass contribution, $M_{\rm total} \sim (1.4\text{–}2.8) \times 10^8\ M_\odot$, is significant for the Galactic baryon budget but does not address the non-baryonic dark matter problem. Future constraints from the Nancy Grace Roman Space Telescope and gravitational wave observations are assessed, with testable predictions quantified.

Keywords: Neutron stars, pulsars, stellar remnants, galactic population, stellar evolution, gravitational microlensing

1 Introduction

Neutron stars are compact remnants formed in core-collapse supernovae of massive stars ($M \gtrsim 8\ M_\odot$). With gravitational masses typically $M_g = 1.2\text{–}2.0\ M_\odot$ (where M_g refers to the gravitational mass as measured by distant observers, distinct from baryonic mass $M_b \approx 1.1 M_g$) compressed into radii $R \approx 10\text{–}13$ km (Choudhury et al., 2024), they exhibit central densities $\rho_c \sim 10^{14}\text{–}10^{15}$ g cm^{-3}. Upon formation, many manifest as pulsars—rotating sources of electromagnetic radiation powered by magnetic dipole spin-down.

The observational census of neutron stars reveals a striking deficit. The ATNF Pulsar Catalogue (Manchester et al., 2005) currently lists ∼3,500 rotation-powered pulsars. However, population synthesis models incorporating Galactic supernova rates of $\mathcal{R}_{\rm SN} \approx 2 \pm 1$ per century (Li et al., 2011; Rozwadowska et al., 2021) and a Galactic age of ∼10 Gyr predict a cumulative neutron star population:

$$N_{\rm NS} \sim \mathcal{R}_{\rm SN} \times t_{\rm Gal} \times f_{\rm NS} \sim (1\text{–}2) \times 10^8 \tag{1}$$

where $f_{\rm NS} \approx 0.5$–0.85 is the fraction of core-collapse events producing neutron stars rather than black holes (Faucher-Giguère & Kaspi, 2006; Sartore et al., 2010). The systematic uncertainty of a factor of ∼2–3 arises from three dominant sources: (1) the slope of the initial mass function at high masses ($\alpha \approx 2.0$–2.7), which affects the core-collapse progenitor rate; (2) variations in supernova rate over Galactic history; and (3) the neutron star retention fraction in the Galaxy, given high natal kick velocities.

This ∼4–5 order-of-magnitude discrepancy between predicted and observed populations implies that $> 99.99\%$ of Galactic neutron stars are undetectable by current methods. These *dormant neutron stars*—objects that no longer emit detectable radiation due to exhaustion of rotational and magnetic energy—represent the dominant but hidden outcome of massive stellar evolution.

This review examines the physical mechanisms leading to dormancy, quantitative detection thresholds, observational constraints from microlensing surveys, and the implications for Galactic mass budgets. We emphasize testable predictions and distinguish between well-constrained physics and model-dependent extrapolations.

2 Physical Mechanisms of Dormancy

2.1 Magnetic Dipole Spin-Down

The rotational energy loss rate for an inclined magnetic dipole is given by (Pacini, 1967; Gunn & Ostriker, 1969):

$$\dot{E} = -\frac{2}{3c^3}|\ddot{\boldsymbol{\mu}}|^2 = -\frac{B_p^2 R^6 \Omega^4 \sin^2\alpha}{6c^3} \tag{2}$$

where B_p is the polar surface magnetic field, R is the stellar radius, $\Omega = 2\pi/P$ is the angular velocity, and α is the magnetic inclination angle. The characteristic spin-down timescale is:

$$\tau_c = \frac{P}{2\dot{P}} \approx 15.8 \text{ Myr} \left(\frac{P}{1 \text{ s}}\right)\left(\frac{\dot{P}}{10^{-15}}\right)^{-1} \tag{3}$$

The cessation of coherent radio emission occurs when the pulsar crosses the "death line" in the P–$\dot{P}$ diagram. The death line arises from the requirement that the potential drop across open field lines exceeds the threshold for electron-positron pair production in the magnetosphere (Ruderman & Sutherland, 1975; Chen & Ruderman, 1993). Without sufficient pair production, the magnetospheric plasma density falls below that required to sustain coherent radio emission. The classical formulation gives:

$$\dot{P} > \dot{P}_{\rm death} \approx 0.17 \times 10^{-15} \; P^2 \text{ s s}^{-1} \tag{4}$$

corresponding to a slope of 2 in log-log space (Chen & Ruderman, 1993). The exact form depends on gap physics assumptions; curvature radiation models yield similar exponents (Zhang et al., 2000).

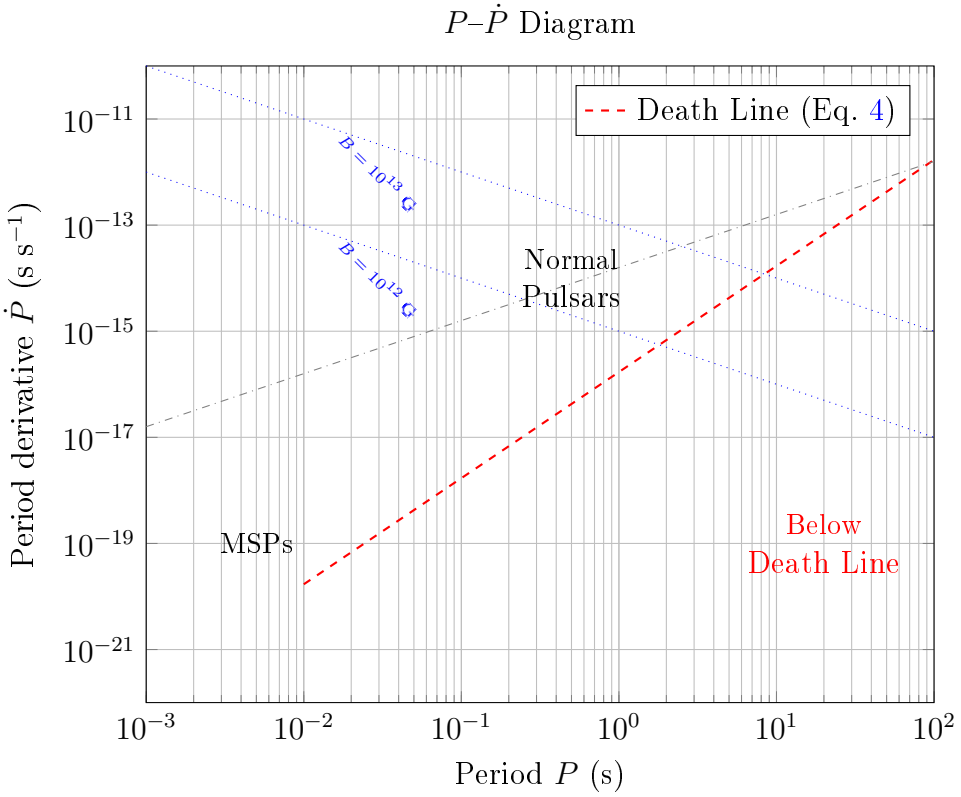

Figure 1: Schematic P–$\dot{P}$ diagram. The red dashed line shows the death line (Equation 4, slope 2 in log-log space), below which radio emission ceases due to insufficient pair production in the magnetosphere. Blue dotted lines indicate constant surface magnetic field ($B^2 \propto P\dot{P}$). Gray dash-dotted line shows constant characteristic age $\tau_c = 1$ Myr. Neutron stars evolve from upper-left toward lower-right, eventually crossing below the death line.

2.2 Magnetic Field Decay and Magneto-Thermal Evolution

The magnetic field evolves through several coupled mechanisms collectively termed magneto-thermal evolution (Viganò et al., 2013; Gourgouliatos & Cumming, 2015). These processes do not operate independently; rather, they form a coupled system where magnetic field evolution affects thermal structure and vice versa.

Ohmic decay operates on a timescale $\tau_{\rm Ohm} \sim L^2/\eta$, where L is the characteristic length scale and η is the magnetic diffusivity, which itself depends on temperature and composition:

$$\tau_{\rm Ohm} \sim 10^6\text{–}10^7 \text{ yr} \left(\frac{T}{10^8 \text{ K}}\right)^2 \tag{5}$$

Hall drift is a nonlinear process that redistributes magnetic energy across length scales with timescale $\tau_{\rm Hall} \sim 4\pi e n_e L^2/(cB)$. For strong fields ($B \gtrsim 10^{13}$ G), Hall drift dominates and can accelerate decay on $\sim 10^4$–10^5 yr timescales. Crucially, Hall drift does

not directly dissipate energy but cascades it to smaller scales where ohmic decay becomes efficient.

Ambipolar diffusion in the core operates on $\tau_{\rm amb} \sim 10^6$–10^7 yr (Goldreich & Reisenegger, 1992), depending on core temperature and composition.

The interaction between these mechanisms creates a feedback loop: magnetic field decay releases heat (Joule heating), which modifies conductivity and thus decay rates. Full magneto-thermal simulations (Viganò et al., 2013) show that this coupling can either accelerate or delay dormancy depending on initial conditions.

Critically, decay timescales vary strongly with initial field strength:

- Magnetars ($B_0 \sim 10^{14}$–10^{15} G): $\tau_{\rm decay} \sim 10^4$–$10^5$ yr
- Normal pulsars ($B_0 \sim 10^{12}$ G): $\tau_{\rm decay} \sim 10^6$–$10^7$ yr

The magnetar catalog (Olausen & Kaspi, 2014) lists ∼30 confirmed magnetars, representing a small fraction of expected magnetar births, consistent with rapid field decay rendering them undetectable within $\lesssim 10^5$ yr.

2.3 Thermal Cooling

Neutron star cooling proceeds through distinct phases (Yakovlev & Pethick, 2004; Page et al., 2006; Potekhin et al., 2015):

1. **Neutrino cooling era** ($t < 10^5$ yr): Core temperature drops from $T_c \sim 10^{11}$ K to $\sim 10^8$ K via neutrino emission. The dominant processes depend on density and composition: modified Urca for standard matter, direct Urca if proton fraction exceeds ∼11–15% (the exact threshold being EOS-dependent, ranging from 11% for stiff EOSs to 15% for soft EOSs).

2. **Photon cooling era** ($t > 10^5$ yr): Surface thermal emission dominates energy loss. Cooling rates depend sensitively on envelope composition (light elements accelerate cooling), superfluidity (which suppresses specific neutrino processes), and equation of state.

The Magnificent Seven (or XDINSs) provide observational benchmarks: with ages $\sim 10^5$–10^6 yr and surface temperatures $T_s \sim 10^6$ K (Haberl, 2007), they represent an intermediate evolutionary stage. The transition timescale from this thermally-luminous state to true dormancy ($T_s \lesssim 10^4$ K) depends on envelope composition but is estimated at $\sim 10^6$–10^7 yr for standard cooling models.

The Cassiopeia A neutron star ($t \approx 340$ yr, $T_s \approx 2 \times 10^6$ K) provides constraints on early cooling (Shternin et al., 2023). NICER observations of active millisecond pulsars provide radius constraints ($R \approx 12$–13 km for $\sim 1.4\ M_\odot$ stars) (Choudhury et al., 2024; Rutherford et al., 2024), but these are active systems, not dormant objects.

2.4 Detection Thresholds

A key quantitative question is: at what temperature does a nearby dormant neutron star become undetectable?

For a blackbody with temperature T_s and radius $R = 12$ km at distance d:

$$F_\nu = \frac{2\pi h\nu^3}{c^2} \frac{1}{e^{h\nu/kT_s} - 1} \frac{R^2}{d^2} \tag{6}$$

At $T_s = 10^4$ K, the spectrum peaks at $\lambda_{\rm peak} \approx 290$ nm (near-UV). The bolometric flux at $d = 100$ pc is:

$$F_{\rm bol} = \sigma T_s^4 \frac{R^2}{d^2} \approx 3 \times 10^{-18} \text{ erg s}^{-1} \text{ cm}^{-2} \tag{7}$$

This corresponds to $V \approx 30$ mag, below optical survey limits. In the mid-infrared at $\lambda = 10$ μm (JWST MIRI F1000W), such a source would have flux density $\lesssim 10$ nJy. For comparison, JWST MIRI achieves $\sim$100 nJy (10σ, 10,000 s) in imaging mode, and $\sim$10 nJy in very deep exposures. Detection would therefore require: (1) prior positional knowledge, (2) extremely deep integrations, and (3) T_s near the upper end of our range.

At $T_s = 3000$ K (the practical lower limit for thermal detectability), $F_{\rm bol}$ drops by a factor of $\sim$100, and the source becomes effectively invisible even to JWST at $d > 10$ pc.

Conclusion: Dormant neutron stars with $T_s \lesssim 10^4$ K at typical Galactic distances ($d \gtrsim 100$ pc) are below current electromagnetic detection thresholds. No candidates have been ruled out by JWST because none have been positionally identified for targeted observation.

3 Population Constraints

3.1 The Observed Deficit

The ATNF Pulsar Catalogue (Manchester et al., 2005) contains $\sim$3,500 pulsars as of late 2025. Correcting for:

- Beaming fraction: Only $f_b \approx 10$–20% of pulsars beam toward Earth (Tauris & Manchester, 1998)
- Survey incompleteness: Selection effects against faint, distant, or high-DM pulsars
- Binary systems not surveyed

The total active pulsar population is estimated at $N_{\rm active} \sim 10^5$–10^6 (Faucher-Giguère & Kaspi, 2006). Comparing with Equation 1:

$$f_{\rm dormant} = 1 - \frac{N_{\rm active}}{N_{\rm NS}} > 99\% \tag{8}$$

3.2 Microlensing Constraints

Microlensing surveys (MACHO, EROS, OGLE) toward the *Magellanic Clouds* provide the most direct constraints on compact object populations in the *Galactic halo*. The optical depth to microlensing is:

$$\tau = \frac{4\pi G}{c^2} \int_0^{D_s} \rho(D_l) D_l (D_s - D_l)/D_s \, dD_l \tag{9}$$

OGLE-IV's 20-year SMC observations found five microlensing events consistent with known stellar populations (disk and SMC self-lensing), with no excess attributable to halo compact objects (Mróz et al., 2024). Combined with LMC results, this constrains:

$$f_{\rm MACHO} \equiv \frac{\Omega_{\rm compact}}{\Omega_{\rm DM}} \lesssim 10\% \text{ for } M \sim 10^{-7}\text{–}10^{3}\ M_\odot \tag{10}$$

Reconciliation with dormant neutron star population: This constraint applies specifically to the *dark matter halo* along lines of sight toward the Magellanic Clouds. Dormant neutron stars, being baryonic, are expected to trace the stellar disk and bulge populations, not the spherical dark matter halo. Microlensing events from disk/bulge neutron stars would be indistinguishable from other stellar lenses in *event rate* (contributing to the known optical depth toward the bulge), though individual events could be distinguished by *mass* via astrometric microlensing.

The Sahu et al. (2022) astrometric microlensing detection of an isolated stellar-mass compact object ($M \approx 7.1\ M_\odot$) toward the Galactic bulge (Sahu et al., 2022) is more consistent with an isolated black hole than a neutron star. However, this detection validates the technique: astrometric microlensing with Gaia and Roman can, in principle, identify dormant neutron stars via their characteristic mass signatures ($M \sim 1.4\ M_\odot$).

3.3 Mass Budget Implications

If $N_{\rm NS} \sim (1\text{–}2) \times 10^8$ dormant neutron stars exist with mean mass $\langle M \rangle \approx 1.4\ M_\odot$:

$$M_{\rm total} \sim (1.4\text{–}2.8) \times 10^8\ M_\odot \tag{11}$$

This is comparable to the stellar mass of the Galactic halo ($\sim 10^9\ M_\odot$) but represents only $\sim$0.1–0.3% of the total Galactic mass ($\sim 10^{12}\ M_\odot$, including dark matter).

Clarification: Dormant neutron stars are *baryonic* and do not address the non-baryonic dark matter problem. Galactic rotation curves require dark matter with total mass $\sim 10^{12}\ M_\odot$, exceeding the neutron star contribution by $\sim$4 orders of magnitude. Dormant neutron stars may contribute to the "missing baryon" problem in galaxies—the discrepancy between predicted and observed baryonic mass—but are fundamentally distinct from dark matter candidates.

4 Observational Evidence and Accretion Physics

4.1 The Magnificent Seven and Related Objects

The seven thermally-emitting isolated neutron stars (the "Magnificent Seven" or XDINSs) demonstrate that some neutron stars remain detectable primarily through residual thermal emission rather than rotational power (Haberl, 2007). With $T_s \sim 10^6$ K and ages $\sim 10^5$–10^6 yr, these represent an intermediate evolutionary stage—still visible, but transitioning toward dormancy over $\sim$Myr timescales.

Distinguishing dormant from radio-quiet neutron stars: Radio-quiet neutron stars (like XDINSs) are detectable in X-rays; truly dormant objects emit no detectable radiation at any wavelength. The Magnificent Seven are *not* dormant—they are radio-quiet but thermally luminous. This distinction is observationally critical.

4.2 Accretion-Induced Reactivation: NGC 7793 P13

The ultraluminous X-ray pulsar NGC 7793 P13 provides direct evidence that quiescent neutron stars can reactivate through accretion. Monitoring from 2011–2024 with XMM-Newton, Chandra, NuSTAR, and NICER revealed (Yoshimoto et al., 2025):

- A faint phase in 2021 with $L_X \sim 10^{38}$ erg s^{-1}
- Rebrightening beginning in 2022
- By 2024, luminosity exceeded 10^{40} erg s^{-1}—more than 100× brighter
- Spin-up rate doubled during rebrightening, indicating enhanced accretion

While P13 is an accreting binary system (not strictly dormant), this demonstrates that neutron stars can transition between low and high states depending on mass supply. A truly dormant isolated neutron star could, in principle, temporarily reactivate if it passed through a dense molecular cloud, though such events would be rare and short-lived.

The 2024 XRISM Resolve observations of GX 13+1 revealed unexpectedly slow winds ($v \sim 280$ km s^{-1}) from a neutron star at the Eddington limit (XRISM Collaboration, 2025). This contrasts with ultrafast outflows ($v \sim 0.2c$) from supermassive black holes, suggesting that accretion disk temperature affects wind acceleration efficiency. While these findings refine our understanding of accretion physics, they do not directly constrain dormant populations and are noted here primarily for completeness in the context of neutron star phenomenology.

5 Testable Predictions

To move beyond model-dependent estimates, the dormant neutron star hypothesis makes the following testable predictions:

1. **Microlensing statistics with Roman Space Telescope**: The Galactic Bulge Time-Domain Survey (launch 2026–2027) will monitor $\sim 2\times10^8$ stars for microlensing over 6 seasons. The expected event rate for a lens population is approximately:

$$\Gamma \sim 2 \times 10^{-5}\ \mathrm{yr}^{-1}\ \mathrm{star}^{-1} \times \left(\frac{N_{\mathrm{lens}}}{10^8}\right) \times \left(\frac{f_{\mathrm{bulge}}}{0.5}\right) \tag{12}$$

   where f_{bulge} is the fraction of neutron stars in the inner Galaxy. For $\sim 10^8$ dormant neutron stars with $f_{\mathrm{bulge}} \sim 0.3$–$0.5$, this predicts ∼10–100 astrometric microlensing events per year with characteristic lens masses $\sim 1.4\ M_\odot$, distinguishable from main-sequence lenses and black holes by mass reconstruction.

2. **Continuous gravitational waves**: An isolated neutron star with ellipticity ϵ spinning at frequency f at distance d produces characteristic strain amplitude at the detector:

$$h_c \approx 4 \times 10^{-27} \left(\frac{\epsilon}{10^{-9}}\right) \left(\frac{f}{100\ \mathrm{Hz}}\right)^2 \left(\frac{1\ \mathrm{kpc}}{d}\right) \tag{13}$$

   Current LIGO sensitivity ($h \sim 10^{-26}$ for continuous waves after long integration) is marginal. Assuming a local density of ∼1 dormant NS per 100 pc^3 and $\epsilon \sim 10^{-9}$, there may be ∼10 sources within 1 kpc detectable by next-generation detectors (Einstein Telescope, Cosmic Explorer) with $h \sim 10^{-27}$ sensitivity.

3. **Transient reactivation**: If dormant neutron stars occasionally pass through dense ISM ($n \sim 10^3$ cm^{-3}), Bondi-Hoyle accretion produces luminosities:

$$L_X \sim 10^{30}\text{–}10^{32}\ \text{erg s}^{-1} \left(\frac{v}{30\ \text{km s}^{-1}} \right)^{-3} \tag{14}$$

Such transients lasting weeks to months should occur at rates $\sim$0.01–0.1 yr^{-1} Galaxy-wide. eROSITA and future X-ray monitors could identify these events, distinguishable from cataclysmic variables by their spectra and lack of optical counterpart.

6 Uncertainties and Assumptions

This review concerns a population whose existence is strongly supported by stellar evolution theory but lacks direct observational confirmation. We distinguish:

Well-established:

- Neutron stars form in core-collapse supernovae
- Pulsars spin down and eventually cross below the death line
- Magnetic fields decay on Myr timescales via well-understood plasma physics
- Thermal emission fades below detection thresholds as stars cool

Model-dependent:

- The precise number (10^7–10^9) depends on supernova rates, retention fractions, and binary evolution
- Spatial distribution depends on birth kick velocities and Galactic potential
- Timescale to complete dormancy depends on poorly constrained microphysics (superfluidity, envelope composition)

Speculative:

- Whether individual dormant neutron stars can be detected with any technique
- Their contribution to unexplained microlensing events
- The frequency of accretion-induced reactivation

Dormant neutron stars share epistemic status with other "indirect" populations in astrophysics (e.g., intermediate-mass black holes, primordial black holes) where theoretical motivation is strong but direct detection remains elusive. The key difference is that the existence of dormant neutron stars follows necessarily from well-established stellar evolution, whereas primordial black holes require additional cosmological assumptions.

7 Conclusion

Dormant neutron stars—stellar remnants that have exhausted rotational and magnetic energy—are a theoretically robust but observationally hidden population. Population synthesis models predict (1–2) $\times 10^8$ such objects in the Milky Way, representing $> 99\%$ of all neutron stars ever formed. Their total baryonic mass ($\sim$ 1–3$\times 10^8$ $M_\odot$) is significant for the Galactic baryon budget but does not solve the non-baryonic dark matter problem.

Current electromagnetic surveys cannot detect isolated neutron stars with surface temperatures $T_s \lesssim 10^4$ K at typical Galactic distances. Microlensing surveys toward the Magellanic Clouds constrain halo compact objects but are consistent with disk/bulge dormant populations. The strongest near-term prospects for detection come from:

1. Astrometric microlensing with Roman Space Telescope ($\sim$10–100 events/yr predicted)
2. Continuous gravitational wave searches with next-generation detectors
3. Transient X-ray monitoring for accretion-induced reactivation

The dormant neutron star population, while invisible, represents a fundamental prediction of stellar evolution theory and a significant component of the Galaxy's baryonic mass budget.

Acknowledgments

The author thanks the anonymous reviewers for detailed feedback that substantially improved the quantitative rigor, clarity, and scientific precision of this manuscript.

References

Chen, K., & Ruderman, M. (1993). Pulsar death lines and death valley. *ApJ*, 402, 264–270.

Choudhury, D., et al. (2024). A NICER view of the nearest millisecond pulsar: PSR J0437–4715. *ApJL*, 971, L20.

Faucher-Giguère, C.-A., & Kaspi, V. M. (2006). Birth and evolution of isolated radio pulsars. *ApJ*, 643, 332–355.

Goldreich, P., & Reisenegger, A. (1992). Magnetic field decay in isolated neutron stars. *ApJ*, 395, 250–258.

Gourgouliatos, K. N., & Cumming, A. (2015). Hall drift and the braking indices of young pulsars. *MNRAS*, 446, 1121–1134.

Gunn, J. E., & Ostriker, J. P. (1969). On the nature of pulsars. III. *ApJ*, 157, 1395.

Haberl, F. (2007). The magnificent seven: Magnetic fields and surface temperature distributions. *Ap&SS*, 308, 181–190.

Li, W., et al. (2011). Nearby supernova rates from the Lick Observatory Supernova Search. III. *MNRAS*, 412, 1473–1507.

Manchester, R. N., Hobbs, G. B., Teoh, A., & Hobbs, M. (2005). The Australia Telescope National Facility Pulsar Catalogue. *AJ*, 129, 1993–2006.

Mróz, P., et al. (2024). Microlensing optical depth and event rate toward the SMC from 20 years of OGLE observations. *ApJS*, 275, 49.

Olausen, S. A., & Kaspi, V. M. (2014). The McGill magnetar catalog. *ApJS*, 212, 6.

Pacini, F. (1967). Energy emission from a neutron star. *Nature*, 216, 567–568.

Page, D., Geppert, U., & Weber, F. (2006). The cooling of compact stars. *Nucl. Phys. A*, 777, 497–530.

Potekhin, A. Y., Pons, J. A., & Page, D. (2015). Neutron stars—cooling and transport. *Space Sci. Rev.*, 191, 239–291.

Rozwadowska, K., Vissani, F., & Cappellaro, E. (2021). On the rate of core collapse supernovae in the Milky Way. *New Astron.*, 83, 101498.

Ruderman, M. A., & Sutherland, P. G. (1975). Theory of pulsars: Polar gaps, sparks, and coherent microwave radiation. *ApJ*, 196, 51–72.

Rutherford, N., et al. (2024). Constraining the dense matter EOS with new NICER mass-radius measurements. *ApJL*, 971, L19.

Sahu, K. C., et al. (2022). An isolated stellar-mass black hole detected with astrometric microlensing. *ApJ*, 933, 83.

Sartore, N., et al. (2010). Galactic population of radio and X-ray pulsars. *A&A*, 510, A23.

Shternin, P. S., et al. (2023). Constraints on neutron star superfluidity from Cassiopeia A cooling. *MNRAS*, 518, 2775–2790.

Tauris, T. M., & Manchester, R. N. (1998). On the evolution of pulsar beams. *MNRAS*, 298, 625–636.

Viganò, D., et al. (2013). Unifying the observational diversity of isolated neutron stars via magneto-thermal evolution. *MNRAS*, 434, 123–141.

XRISM Collaboration. (2025). Stratified wind from a super-Eddington X-ray binary. *Nature*, 635, 1132–1136.

Yakovlev, D. G., & Pethick, C. J. (2004). Neutron star cooling. *ARAA*, 42, 169–210.

Yoshimoto, M., et al. (2025). Monitoring NGC 7793 P13: Spectral and timing properties. *ApJL*, 993, L26.

Zhang, B., Harding, A. K., & Muslimov, A. G. (2000). Radio pulsar death line revisited. *ApJL*, 531, L135–L138.